University of Groningen

A comparison of the electrical properties of polymer LEDs based on poly(thiophene)s and PPV-derivatives

Garten, Frank

IMPORTANT NOTE: You are advised to consult the publisher's version (publisher's PDF) if you wish to cite from it. Please check the document version below.

Document Version
Publisher's PDF, also known as Version of record

Publication date:
1998

[Link to publication in University of Groningen/UMCG research database](#)

Copyright
Other than for strictly personal use, it is not permitted to download or to forward/distribute the text or part of it without the consent of the author(s) and/or copyright holder(s), unless the work is under an open content license (like Creative Commons).

The publication may also be distributed here under the terms of Article 25fa of the Dutch Copyright Act, indicated by the "Taverne" license. More information can be found on the University of Groningen website: https://www.rug.nl/library/open-access/self-archiving-pure/taverne-amendment.

Take-down policy
If you believe that this document breaches copyright please contact us providing details, and we will remove access to the work immediately and investigate your claim.

Downloaded from the University of Groningen/UMCG research database (Pure): http://www.rug.nl/research/portal. For technical reasons the number of authors shown on this cover page is limited to 10 maximum.

Download date: 06-06-2022

Chapter 4

Poly(3-octylthiophene)-based LEDs;
...from red...

Abstract
The dominant role of the cathodic injection process in poly(3-octylthiophene) (P3OT)-based LEDs is described. The non-uniform field distribution in an ITO/P3OT/Al device structure is a result of significant band bending at the cathode, associated with Schottky barrier formation. The unique observation of EL under reverse bias conditions is a result of different carrier injection processes for both charge carriers at the electrodes, leading however to the same kind of excited states responsible for EL in P3OT. Changing the workfunction of the top electrode by only 0.9 eV results in an effective difference in rectification ratios of 6 orders of magnitude. Maximum internal EL efficiencies up to 0.16 % for P3OT-LEDs were realised by reduction of the cathodic injection barrier to almost 0 eV by using a Ca top contact.

In this chapter, LEDs with P3OT are described in terms of the universally applied band picture. In this picture, a uniform field distribution (hence a completely depleted polymer film) gives rise to straight bands representing the polymer HOMO- and LUMO-levels. Deviations from the LED characteristics of PPV-based devices usually described within the framework of this band picture are attributed to the high acceptor concentration N_A in the films. This naturally leads to a non-uniform field distribution across the organic film as a consequence of the presence of a depletion zone at the metal/polymer electrode(s). A modification of the standard band picture is presented for polymeric LEDs in which the active layer initially has a high background carrier concentration.

4.1 Fabrication

All devices described in this chapter and most devices in the next two chapters are based on single-layer structures, consisting of a polymer film sandwiched between electron- and hole injecting contacts. Glass slides covered with a thin conducting film of Indium Tin Oxide (ITO) (Balzers AG) are used as the transparent hole-injecting contact. P3OT was prepared via a regioselective polymerisation procedure (see section 3.5), which provides the possibility to tune the wavelength of light emission in the visible regime by chemically adjusting the position of sterically interacting sidegroups on the main-chain backbone [1]. The desired regioselectivity was confirmed by ^{1}H-NMR spectroscopy. The polymer

was purified by repeated precipitation prior to use. When the conjugation length is not intentionally blocked by the introduction of head-to-head instead of head-to-tail interacting sidegroups, this conjugated polymer emits in the red part of the visible spectrum. The material is very well soluble in common organic solvents like toluene, xylene and chloroform. Here, the active material is spin-coated from a 3-5%-solution in toluene at rotation speeds of 500-4000 rpm. Prior to spin-coating the ITO-surfaces are properly cleaned using a self-developed procedure based on rinsing in de-ionised water and ultrasonic rinsing in polar and non-polar solvents. The polymer solution is filtered using 0.2 μm filters (Spartan 13/30, Schleicher and Schuell). The obtained film thicknesses are measured with a Dektak 3130 surface profiler, and vary between 30 and 200 nm.

Homogeneous layers with a surface roughness of less than 5 % of the film thickness are obtained from the polymer, as was confirmed by optical inspection and Atomic Force Microscopy (AFM) scans. Since temperature-induced crystallisation is known to occur in P3OT-films within a day after preparation, the solvents were removed at temperatures not exceeding 50 degrees. With this procedure no crystallisation effects will occur within the first days after processing. Top electrodes of 80-150 nm thickness are made by thermal evaporation of Al through a mask at pressures below $2 \cdot 10^{-8}$ Torr and with a deposition rate not exceeding 1 nm/s. The electrode area of the device varies from 8 to 24 mm^2; these electrodes were contacted in a specially designed sample holder with Au spring contacts.

Electrical characterisation of the devices was performed with a Keithley 236 Source Measure Unit (SMU), operated either in pulsed mode with low duty cycle (t_{on} = 100 ms, t_{off} = 900 ms, to avoid heating effects at higher voltages and currents) or in continuous mode (to minimise total measurement time). For polymers which can only be operated at high electric fields the pulsed mode was always applied, to reduce heat development. Capacitance-Voltage (CV)-measurements are performed at 1 kHz with a HP4275 semiconductor-analyser. LV-characteristics and external quantum efficiencies can be obtained during standard electrical characterisation, as the device is mounted on an integrating sphere. The light intensity L is measured with a calibrated photodiode in a 90 degree configuration using an SR-400 photon counter in combination with the SMU.

In this Chapter the fabrication of a batch of P3OT-LEDs of 8 samples with different polymer film thicknesses and 7 top electrodes on each sample made it possible to relate the electrical characteristics to the film thickness, and to judge the reproducibility of the results. As device performance is strongly related to seemingly unimportant details in the fabrication procedure (clean glassware, baking temperatures after spincoating, spinning time, time-lag between spin-coating and evaporation of the top electrode) a quantitative comparison of the electrical data from sample to sample is generally difficult. Within one sample, however, a high degree of reproducibility is obtained, although especially in
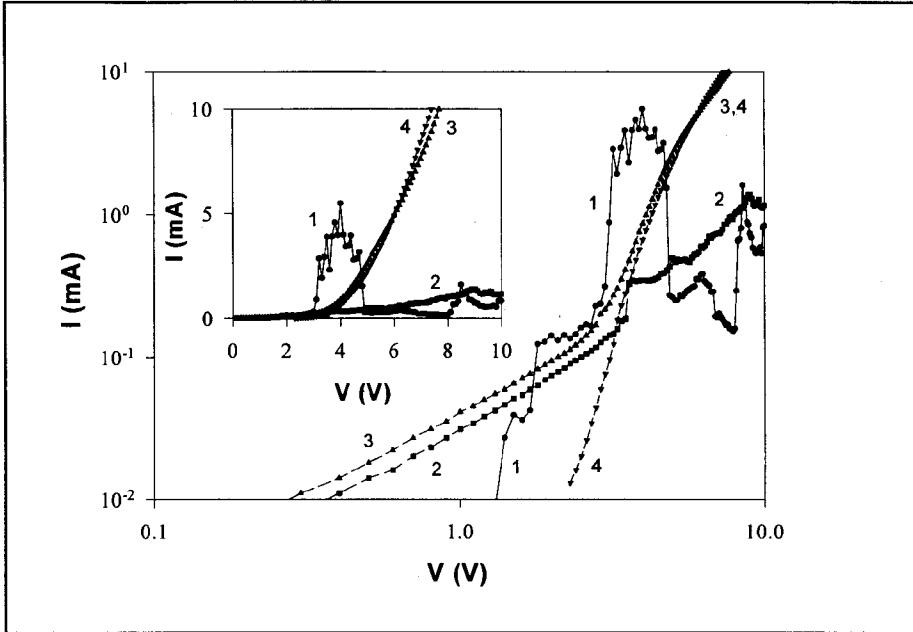
Fig. 4.1   *IV-characteristics of the first 4 consecutive measurements on an ITO/P3OT/Al structure. The inset shows the same data on linear scales.*

devices with thin active layers (< 60 nm) the chance for short circuits is substantially increased.

For most of the tested devices the first measurements show an irreproducible and spiky characteristic. This is shown in Fig. 4.1 where the *IV*-characteristics (pulsed mode of operation) of a typical diode are shown on a log-log scale for 4 subsequent measurements; the inset shows the same data on a double linear scale. While initially irregular and spiky characteristics are obtained (1 and 2), after a few measurements the IV becomes regular, and is reproducible for each subsequent measurement (3 and 4). From this moment on any parallel conductance resulting from weak local shorts does not play a role any longer, as can be seen from the log-log plot. The initial low-voltage line is attributed to shorts ($I \propto V$), while in the fourth measurement the current depends exponentially on the applied voltage V. All *IV*-characteristics reproduced in this thesis are taken after regular, reproducible characteristics have been obtained.

4.2 Electrical properties of single-layer P3OT LEDs

A remarkable difference between PPV-based and thiophene-based LEDs is the influence of the total film thickness of the active layer on the IV and LV characteristics. In the case of most PPV-based devices the operation voltage of the devices (which is defined as the voltage required to reach a particular current density through the LED) scales with the film thickness. This relation was clearly demonstrated by Parker [2], who showed that a plot of the current-density J vs. the electric field E ($E = V/d$, in which d is the film thickness) is independent of the thickness d. A straightforward conclusion is that the electric field is uniformly distributed across the polymer film, which is supported by a rigid band structure without band bending effects at the interfaces.
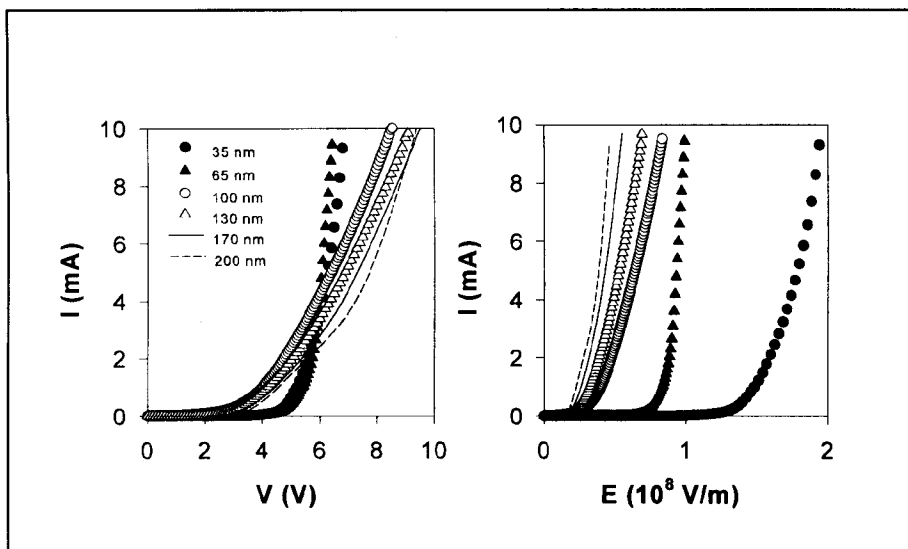

Fig. 4.2   *IV-characteristics   (left)   and   IE-characteristics   (right)   for ITO/P3OT/Al devices, for 6 different thicknesses of the polymer film. The electric field E in (b) is defined as the voltage divided by the thickness of the film.*

This thickness dependence does not apply to P3OT-based devices, as is demonstrated in Fig. 4.2. Here the *IV*-characteristic (Fig. 4.2 a) and the IE-characteristic (Fig. 4.2 b) are plotted for single-layer device structures with thicknesses varying from 35 to 200 nm thickness. These different thicknesses were obtained by systematic variation of the spin coating rotation speed and the concentration of the polymer solution.

The operation voltage of an ITO/P3OT/Al structure is independent of the total thickness of the polymeric semiconductor, for devices with a thickness of 100 nm or more. This naturally leads to the conclusion that the field-distribution across the device is not uniform, and that the field strength is higher at one of the electrodes than the field in the bulk of the polymer film. This picture is justified by the plot of J vs. E, which shows that not an average electric field V/d but an absolute voltage V is required to establish a certain current density through the LED. The deviations from this picture occur at smaller film thicknesses (35 and 65 nm); in very thin devices a much higher average electric field is required to reach a particular current density. From CV-measurements (end of this section) it can be concluded that a 100 nm-thick device is depleted over a region of 49 nm of the total film thickness. This depletion width w depends on the carrier background concentration N_A in the pristine film and the build-in voltage V_{bi}, as is expressed by Eq. 4.5. Since these parameters are independent of the device thickness, we conclude that for this polymeric material with these particular electrodes a space charge zone of 49 nm extension needs to be established to compensate for the Fermi-level offset between the metal and the polymer. Conclusively, a 35-nm thick device will be fully depleted, as is reflected experimentally by a higher average electric field at a particular current density for thin devices. This observation is in strong contrast to all thickness-dependent studies of polymeric LEDs with a PPV-derivative as the active semiconducting layer, and indicates that P3OT-LEDs behave intrinsically different from PPV-based devices. It is important to note here that this observation cannot necessarily be generalised for devices based on other poly(thiophene)-derivatives with different carrier background concentrations, and that also PPV-derivatives with high enough acceptor densities may be partially depleted (form Schottky contacts) when contacted with a metallic electrode [3-5].

A dominant voltage drop at one of the electrodes of an ITO/P3OT/Al structure results from band-bending at the electrode, which requires a modification of the rigid-band model introduced by Parker and described in section 2.3. The strong band bending at anode or cathode in combination with the non-uniform field distribution across the LED leads to a description of a metal/P3OT-contact in terms of the standard Schottky theory for metal/semiconductor contacts. The first description of a metal/poly(3-alkylthiophene) (P3AT)-contact in terms of a Schottky contact between a metal and a p-type semiconductor was proposed already in 1987 by Tomozawa *et al.* [6].

When a very high-workfunction electrode ITO is brought into contact with the p-type semiconductor P3OT, electrons will flow from P3OT into the anode in order to obtain charge equilibrium. This results in a positive space charge zone in the polymer close to the contact and band bending as indicated in Fig. 4.3. In practice, however, the ITO/P3OT barrier for holes is so small ($\phi_{b,h} = I_p - \chi_s = 5.0 - 4.8 = 0.2$ eV) that it can be treated as an Ohmic contact, where holes can pass the barrier already when locally a low electric field is established. In Fig. 4.3 the workfunctions of two metal electrodes for an ITO/P3OT/Al device are given in
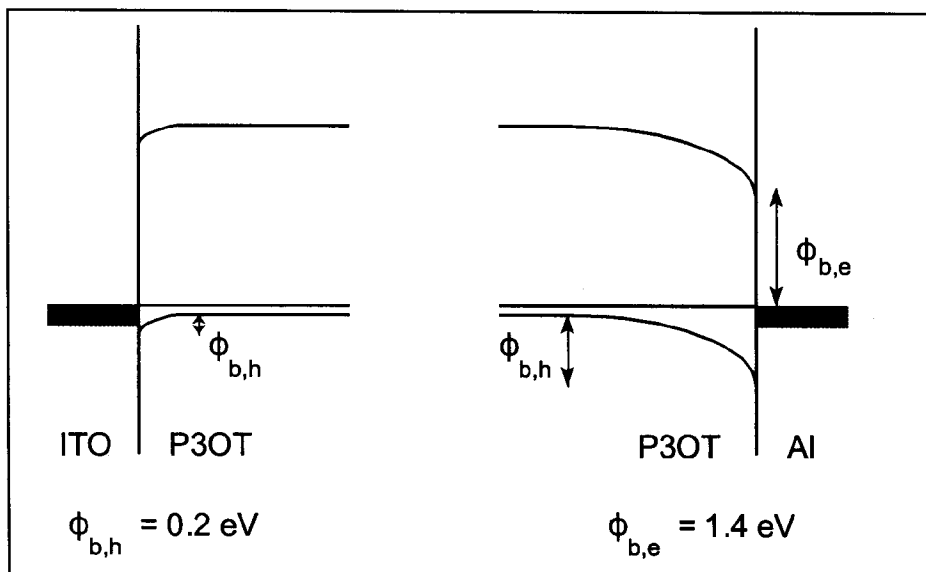
Fig. 4.3 *Schematic representation of band-bending at the anode (ITO/P3OT) and the cathode (P3OT/Al).*
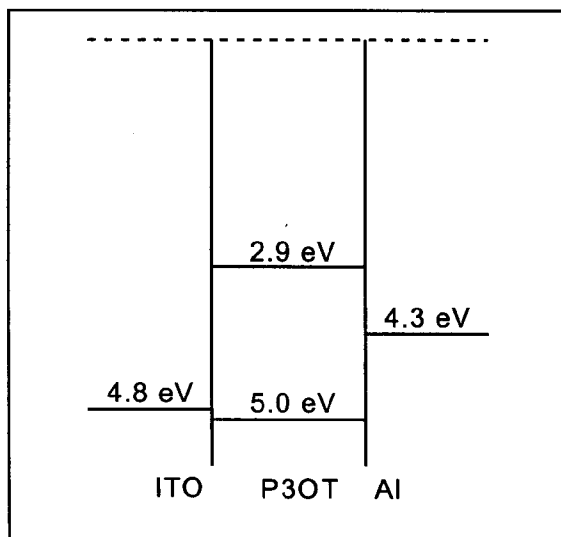
Fig. 4.4 *Energetic positions of the molecular HOMO and LUMO levels of P3OT in relation to the Fermi-level positions of the metallic electrodes ITO and Al.*

relation to the representative energy levels for P3OT. The workfunctions for ITO and Al are average values based on handbook tables and literature reports, which yield ($\phi_{m,ITO}$ = 4.8 eV and ($\phi_{m,Al}$ = 4.3 eV.

The opposite situation occurs at the Al/P3OT electrode, where an electron-injection barrier $\phi_{b,e}$ = ϕ_s - χ_s = 4.3 - 2.9 = 1.4 eV is established at charge equilibrium. This situation is obtained as a consequence of the flow of electrons from the Al electrode into the semiconducting polymer film, establishing a hole-depletion zone in P3OT at the cathodic interface. A barrier of 0.7 eV for holes drifting from the polymer layer into the metal contact is established as a direct result of the interfacial band bending.

When a positive voltage is applied across the Al/P3OT contact (the positive voltage is applied to the ITO contact while the Al contact is grounded) two contributions to the total current are established: a drift current J_{dr} of electrons in the strong electric field across the depletion zone, and a diffusion current J_D the other way around. The total current density J at the contact becomes:

$$J = J_S [\exp (q\,V / n\,k_B\,T) - 1], \tag{4.1}$$

and

$$J_S = A^{**}\,T^2 \exp (- q\,\phi_b / k_B\,T). \tag{4.2}$$

Here J_S is the saturation current density, V is the applied voltage, n is the ideality factor (equal to 1 for an ideal Schottky contact), ϕ_b is the Schottky barrier height, and A^{**} is the so-called effective Richardson constant. For an electron in free space its value is 120 Acm^{-2}K^{-2}. The expression $\exp (- q\,\phi_b / k_B\,T)$ (Boltzmann factor) reflects the fraction of charges in the metal or semiconductor able to overcome the Schottky barrier by thermionic emission at a specific temperature T.

In Fig. 4.5 the current density J is replotted as a function of the applied voltage V on a semilogarithmic scale. Below the onset of electroluminescence (EL) in the low voltage regime an exponential behaviour is obtained, as would be expected in line with Eq. 4.1. Extrapolation to V = 0 yields J_S and hence the Schottky barrier height ϕ_b via Eq. 4.2: ϕ_b = 0.69 eV. This value is in close agreement to the values for similar P3AT-based contacts to Al reported in the literature [6,7]. The ideality factor n is obtained from the slope of log J vs. V at low voltage: n = 2-7. This ideality factor is observed to vary quite a lot from sample to sample. However, it is always > 2 and highly reproducible for several devices on one sample. The deviations of n from the ideal value 1 are characteristic for Schotty-contacts with organic semiconductors [6,8], and reflect the discrepancy between standard thermionic emission/diffusion models and the details of carrier injection into thiophene-based semiconductors. This may result from a variety of reasons,

such as a more pronounced influence of traps in disordered organic conductors, and the formation of insulating interface layers upon oxidation of the top contact and of the top of the film prior to metallisation.
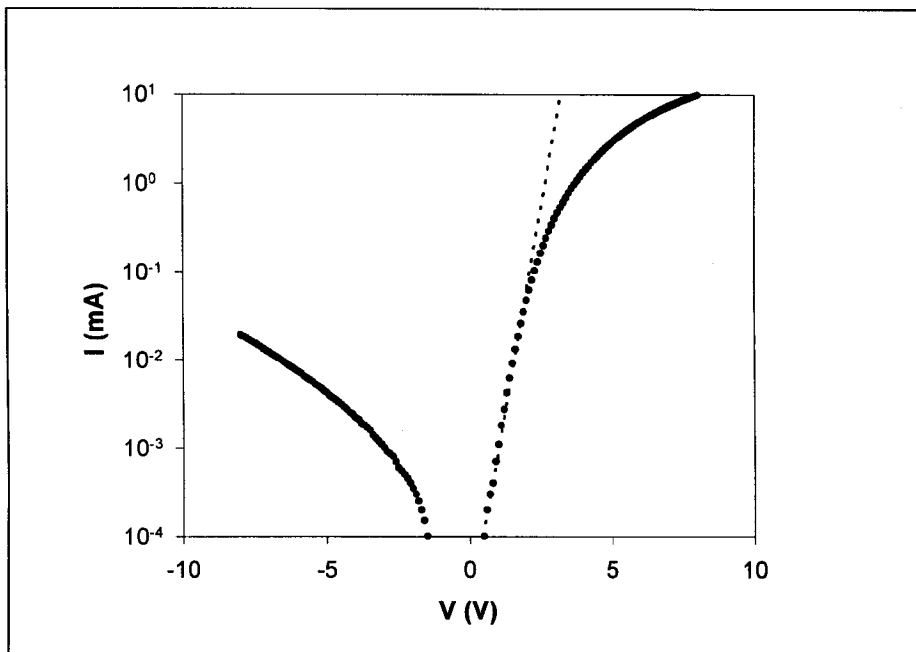

Fig. 4.5   *Semi-logarithmic plot of the forward and reverse JV-characteristics of an ITO/P3OT/Al device. The dotted line is a guide to the eye, emphasising the exponential dependence of the current on the applied forward bias at low V.*

The barrier ϕ_b is the barrier that holes face when transported across the P3OT LED to the Al electrode. This value is in excellent agreement to the estimate based on the values of the Al workfunction and the energy gap. From these a barrier of 0.7 eV was calculated for holes leaving the polymer film and moving into the Al electrode.

An independent way to establish the existence of a depletion zone at a Schottky contact is to measure the capacitance of such a contact as a function of the applied reverse bias voltage. The capacitance C of the depleted zone at a Schottky contact between a p-type semiconductor and a metal with Schottky barrier height ϕ_b depends on the applied voltage V as:

$$C = A \left[\left(q \, \varepsilon_s \, N_A / 2 \right)^{1/2} \left(V_{int} - V \right)^{-1/2} \right],$$ (4.3)

in which V_{int} is the intercept voltage of the junction ($V_{int} = V_{bi} - (k_B T / q)$ in which V_{bi} is the build-in potential and ($k_B T / q$) is the thermal potential), ε_s is the dielectric constant of the semiconductor, A is the total cross-sectional area of the contact and N_A is the density of ionised acceptor sites present in the P3OT-film.
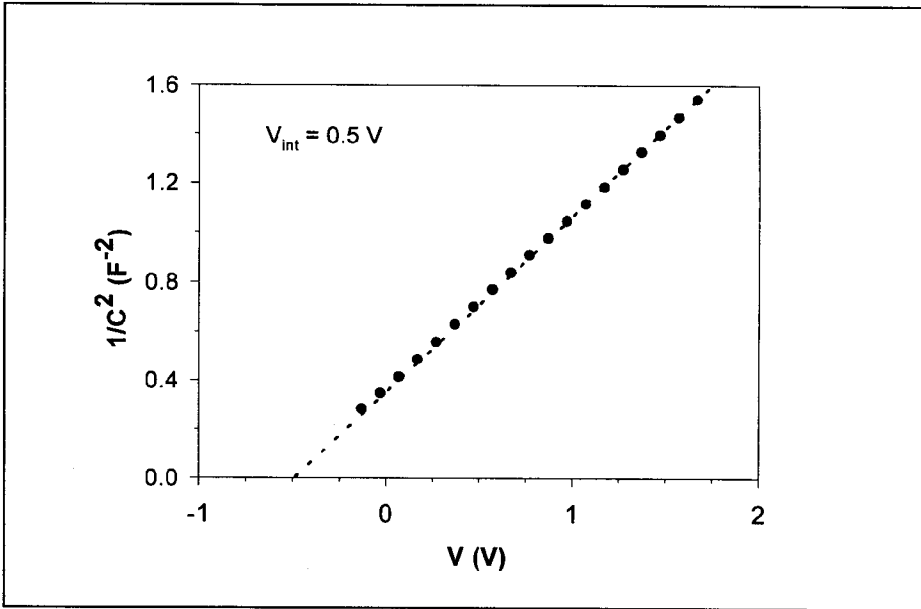
Fig. 4.6   *Reverse bias CV characteristics of an ITO/P3OT/Al device, the capacitance plotted as 1/C^2. The dotted line crosses the x-axis at V=-0.5 V, which corresponds to V_{int}.*

A measurement of (1 / C^2) as a function of the reverse voltage V is presented in Fig. 4.6 and a straight line can be fitted to the data at low reverse bias, as would be expected based on Eq. 4.4:

$$1 / C^2 = \left(2 / q \, A^2 \, \varepsilon_s \, N_A \right) \left(V_{bi} - V - (k_B T / q) \right).$$ (4.4)

According to this equation the intercept with the V axis is at $V_{int} = V_{bi} - (k_B T / q)$ which yields a build-in voltage of 0.5 V. This value is in reasonable agreement with the value found by Tomozawa *et al.* [6] for In/P3HT-contacts [P3HT =

poly(3-hexylthiophene), which is analogous to P3OT except for the length of the alkyl-substituent at the 3-position; the workfunction of In is equal to that of Al, $\phi_{m,In}$ = 4.3 eV].

The slope of the straight line at low bias (Eq. 4.4) yields the acceptor density N_A, provided that the dielectric constant of the semiconductor is known. The acceptor density N_A for a P3OT/Al contact yields N_A = 7.9·10^{16} cm^{-3}, in-line with commonly reported values for P3AT-contacts [6,9]. The zero-bias width w of the depletion layer is given by

$$w = [\, (\, 2 \, \varepsilon_s \, / \, q \, N_A \,) \, V_{bi}^{\frac{1}{2}} \,],$$ (4.5)

and yields 49 nm for the P3OT/Al Schottky contacts described. The fact that the width of the depletion zone is relatively large in relation to the total device thickness of 100 nm supports the insensitivity of the *IV*-characteristic to the total device thickness, which is a result of a non-uniform voltage distribution across the device.

It is generally observed that the CV-characteristics reported here (and in general in the literature) show a lower degree of reproducibility than the *IV*-characteristics. This is believed to be a consequence of the chemical details of the metal/polymer contact, where the impurity concentration N_A does not only have an intrinsic but also an extrinsic contribution as a result of contamination from the electrodes [10]. This results in a non-uniform N_A throughout the depletion zone, hence a curved $1/C^2$ vs. V [5].

Also, it should be mentioned at this point that the nature of the dopants identified by CV-measurements is not unequivocal. Although a direct relation of the acceptor concentration N_A to the presence of residuals remaining from the synthesis is quite feasible, there are literature examples of very-well cleaned oligomer samples (effective chemical and thermal cleaning, in which evaporation under vacuum is the final step) with still very high dopant concentrations [11]. Since also the presence of oxidants and other chemical contaminations is known to contribute to the acceptor density N_A, more detailed investigations are needed to identify the nature of the states that play a role in the CV-measurements described.

The representation of an ITO/P3OT/Al device as a Schottky diode has been justified in the literature by using another powerful method called 'complex impedance spectroscopy', which separates bulk and interfacial contributions to the electrical behaviour of the device. Following this approach, the device is represented by an equivalent circuit (Fig. 4.7), in which R_j and C_j characterise the resistance and the capacitance of the Schottky junction, while R_b and C_b represent the undepleted bulk. The general technique is to apply a sinusoidal voltage signal $v(t) = V_m(t) \sin (\omega t)$ to the device, and to analyse the phase-
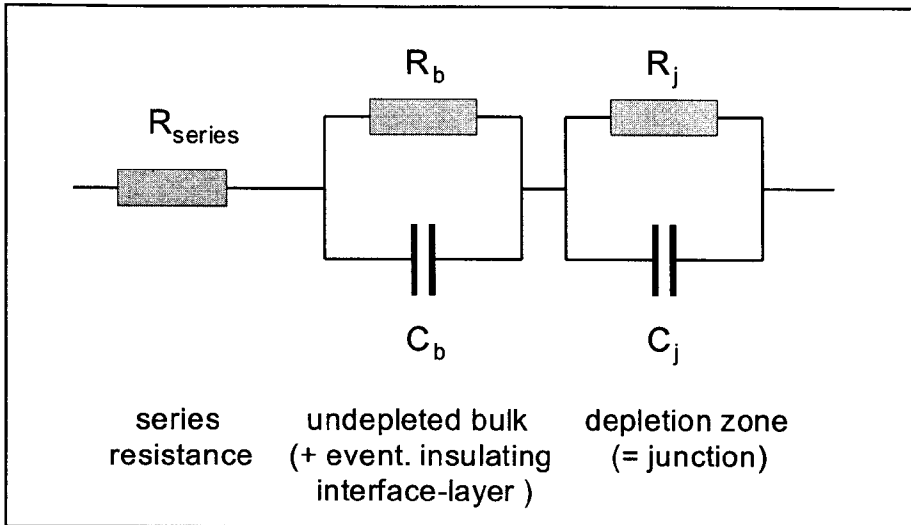
Fig. 4.7 *Schematic representation of a polymeric LED by its equivalent circuit, containing a series resistance and two R-C units corresponding respectively to the impedance of the undepleted bulk and the depletion zone.*

shifted current response $i(t) = I_m(t) \sin(\omega t + \Theta)$. The complex impedance $Z(\omega)$ is defined as

$$Z(\omega) = v(t) / i(t), \tag{4.6}$$

which for the circuit of Fig. 4.7 can be re-written as

$$Z(\omega) = R_{series} + [R_j / (1 + j \omega R_j C_j)] + [R_b / (1 + j \omega R_b C_b)]. \tag{4.7}$$

The complex-impedance plot of such a circuit consists of slightly overlapping semi-circles, translated from the origin by the series (contact) resistance R_{series}; the idealised plot (so-called 'Cole-Cole plot') is indicated in Fig. 4.8. In this plot R_{series} is the resistance associated with current transport through the metallic electrodes, R_b represents the resistance of the undepleted part of the bulk and an eventual insulating interfacial layer, while R_j represents the resistance of the depletion region of this Schottky contact.
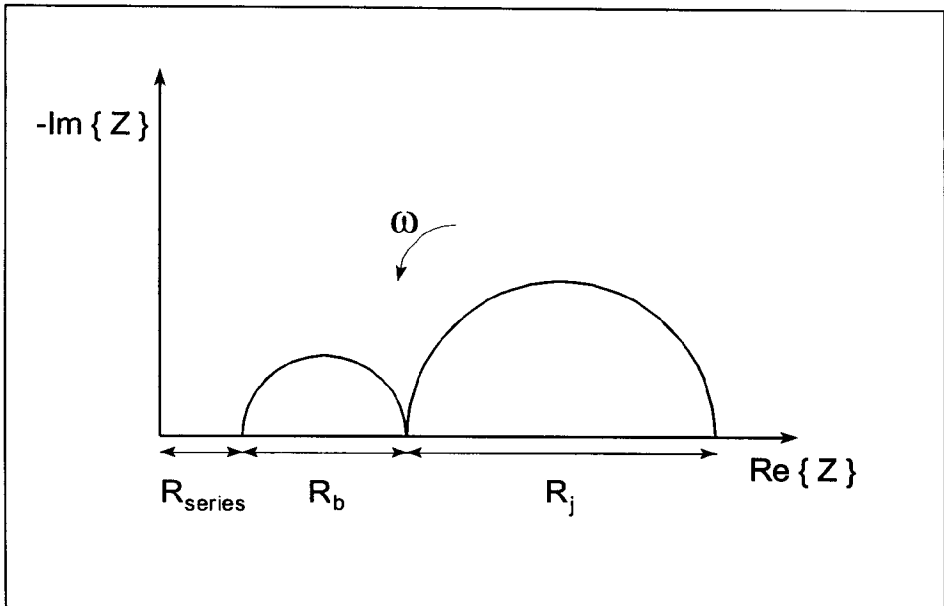
Fig. 4.8   *Cole-Cole plot of the complex impedance of the electrical circuit of Fig. 4.7, in which the two semi-circles are the contributions of the undepleted bulk and the depletion zone.*

Experimental data [3,12-14] confirm that the semi-circle represented by R_j and C_j corresponds to the junction of the device; under increasing forward bias the radius of the semi-circle decreases as a result of the changing width of the depletion zone. The resistance of the undepleted bulk does not depend on the applied bias, and the corresponding semi-circle disappears for lower frequencies; only the junction-contribution remains.

The presence of a P3OT/Al Schottky contact, as has been confirmed by IV and CV characterisation as well as complex impedance spectroscopy, has only been reported for P3AT-based devices [15]. In contrast, most PPV-based LEDs show complete depletion throughout the whole polymer structure, which is experimentally confirmed by a voltage-independent capacitance [13]. This intrinsic difference between P3OT-based and PPV-based devices is entirely attributed to the carrier background concentration N_A in the semiconductor. The conclusion that the presence of charged impurities in the film does contribute to the width of a depletion zone at the contact is not new. The way presented here, however, directly relates this acceptor density N_A responsible for the non-uniform field distribution to the behaviour of the *IV*-characteristics (especially the thickness-dependence). The dopant concentration in P3AT-based devices [9] is generally a few orders of magnitude higher than in PPV-based devices [3,13,16],

which is mainly caused by the presence of $FeCl_3$ residuals in the film from the oxidative coupling reaction used for the chemical synthesis of P3OT. $FeCl_3$ is known to be an acceptor dopant for poly(thiophene)s, hence increasing N_A in the film.

4.3 Reverse-bias electroluminescence in ITO/P3OT/Al LEDs
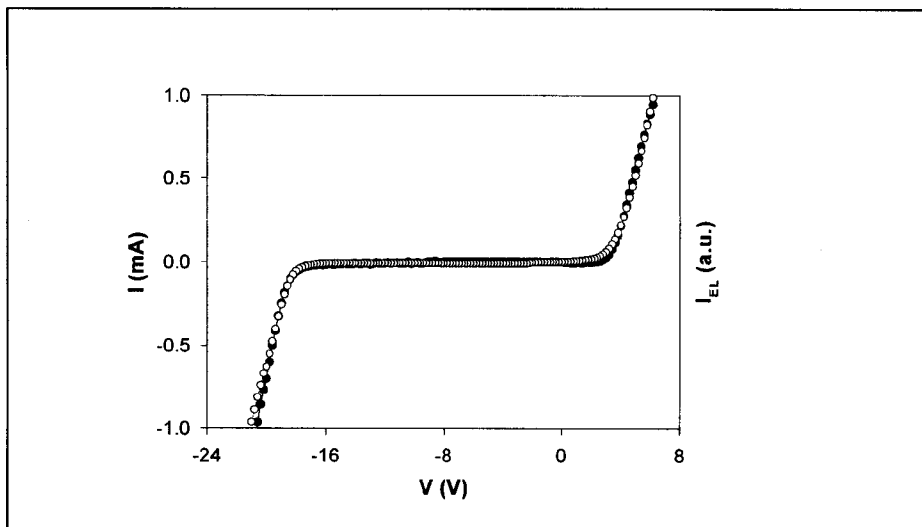
Fig. 4.9 *IV and LV-characteristics of an ITO/P3OT/Al LED, showing EL at low forward and high reverse bias fields.*

Fig. 4.9 represents the *IV-* and LV-characteristics of an ITO/P3OT/Al structure under forward as well as reverse biased conditions. Under reverse bias conditions the positive polarity corresponds to the low-workfunction metallic electrode (Al). The strong asymmetric character of the curve indicates the dominant role of the P3OT-metal interfaces, since a bulk-controlled current density would result in a symmetric characteristic. From the logarithmic representation shown in Fig. 4.5 a rectification ratio between the two current directions of almost 4 orders of magnitude was obtained. In-line with the previous statement that P3OT/ITO contacts behave as Ohmic contacts compared to P3OT/Al (Schottky contacts, exhibiting injection-limited current densities) the high rectification ratio of the ITO/P3OT/Al structure is a direct result of the rectifying properties of the P3OT/Al Schottky contact.

The rectification is covered by Eq. 4.1 if the condition $J_S \ll J$ has been met, i.e. the current resulting from thermionic emission of charge carriers over a barrier ϕ_b is negligible compared to the forward-biased hole current from the semiconductor into the Al electrode. This condition is always met at experimental conditions when $V > 0$ V.

Above the turn-on voltage of the device the current density J consists of two contributions:

$$J = J_h + J_e, \tag{4.8}$$

in which J_h is the hole current flowing from ITO via P3OT into the Al contact, and J_e is the electron current injected from Al into P3OT ($\phi_b = 1.4$ eV). The electron contribution, however, is small compared to J_h, as a result of the high electron injection barrier and the low electron mobility in P3OT. At voltages required to inject the first electrons across the barrier ϕ_b, the hole current J_h dominates the total current density J, as a consequence of the Ohmic character of the opposite ITO/P3OT electrode and the relatively low barrier for holes at the P3OT/Al contact. The rectifying properties of an ITO/P3OT/Al structure are reflected directly by the imbalance of the hole-currents under forward and reverse bias conditions, since the electron contribution plays a negligible role in the overall current in both modes of operation.

At higher reverse bias voltages across the LED, the band picture of Fig. 4.3 is modified such that the effect of band bending at the Al/P3OT interface present at $V = 0$ V becomes negligible. Under high-field conditions the bands are almost straight, resulting in a continuous voltage drop across equal parts of the P3OT-film (uniform electric field). Under these experimental conditions a relatively large hole-current flows through the device, while the injection of electrons is negligible at the ITO/P3OT interface. Only at very high electric fields ($E = 1.8 \cdot 10^8$ V/m), electron injection into the polymer film is achieved, as is manifested by the onset of EL beyond this field. The observation of reverse bias EL in conjugated polymer LEDs is completely unique to this field of research, and has only been reported in symmetric PPV-based devices with relatively low turn-on fields.

The injection mechanism of charge carriers from the electrodes into the transport bands of the polymer is completely different from the dominating mechanism in the forward mode of operation, as is justified by the different turn-on fields and the details of band alignment at the metal/polymer interfaces. The detailed plot of the band model representation of the ITO/P3OT interface at high reverse bias conditions is given in Fig. 4.10, indicating that at those high electric fields the dominant injection mechanism should be direct tunnelling of charge carriers into the polymer bands. In strong contrast to PPV-based LEDs with almost symmetric LV-characteristics (see section 6.1), ITO/P3OT/Al LEDs exhibit an onset of EL at completely different electric fields, as a consequence of different carrier injection mechanisms at both electrodes of the device.
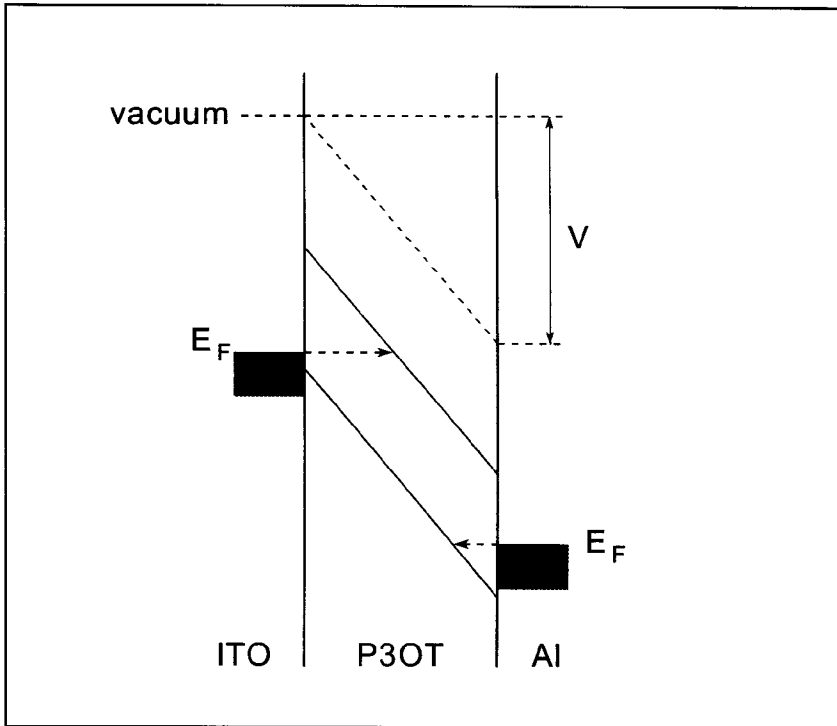
Fig. 4.10 *Schematic representation of the energy bands of P3OT in a reverse-biased ITO/P3OT/Al-structure, tilted as a result of the high electric fields across the device. The dotted arrows schematically indicate the tunnelling paths for carriers to enter the polymer transport bands directly.*

Since tunnelling of charge carriers into the polymer films under reverse bias conditions should be a field driven process, the onset of EL in this mode of operation is expected to be associated with the experimentally determined electric field E of $1.8 \cdot 10^8$ V/m. Hence the onset voltage of EL under reverse bias should scale with the film thickness of the active layer, in contrast to the onset of EL in forward mode (see Fig. 4.2). In Fig. 4.11 this behaviour is illustrated for P3OT-based LEDs with 6 different thicknesses of the active semiconducting film. Only for the thinnest films deviations from the field-dependence are observed, showing that a higher average electric field is required to establish a particular current density through the device. These deviations cannot be attributed to the fact that the depletion zone extends beyond the film thickness, since at high reverse voltages the film is depleted anyway. A relatively large error in the film thickness for a very thin device in combination with an enhanced influence of
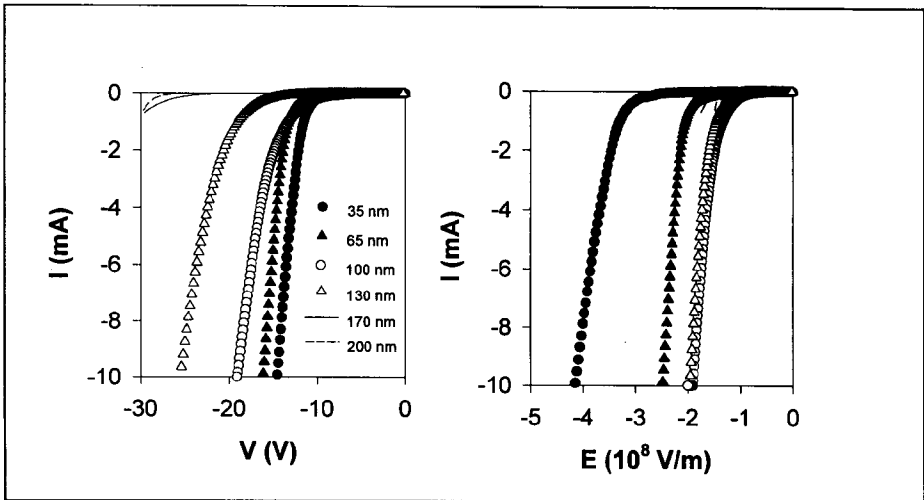
Fig. 4.11 *Reverse-bias IV and IE-characteristics of ITO/P3OT/Al-devices, with varying thicknesses of the P3OT-film. The electric field is defined as the voltage divided by the polymer thickness.*

irregular non-uniform interface-profiles along the device cross section are believed to be primary responsible for these low-thickness deviations.

The quantum efficiency of the recombination process under reverse bias conditions is usually slightly higher than the forward-mode efficiency of the LED, although the difference is small and hardly noticable at low currents (see Fig. 4.9). This is likely to be a consequence of the more balanced contributions of electrons and holes to the total current density in the reverse mode. The rectification observed for ITO/P3OT/Al indicates that the reverse bias hole current is significantly reduced compared to the normal mode of operation. At the onset of electron injection under reverse bias conditions the recombination zone will extend through the active polymer film and will not be limited to a small region close to one of the contacts. A secondary effect that enhances the efficiency under these conditions is that the main recombination zone is spatially separated from the metallic contact, resulting in reduced exciton quenching at the cathode.
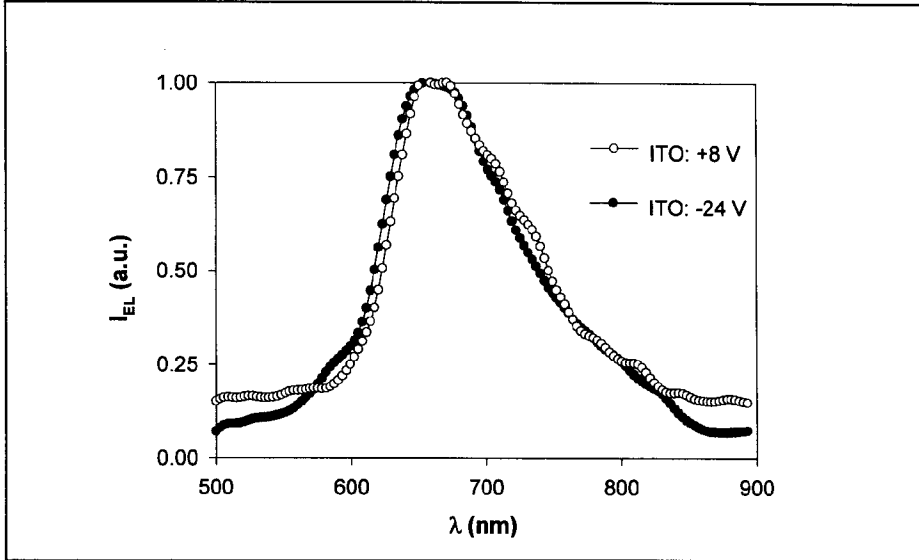
Fig. 4.12   *EL-spectra of an ITO/P3OT/Al-device, at forward (+8 V) and reverse (-20 V) bias.*

The reverse bias EL is of the same excitonic origin as the forward bias luminescence, proving that the same excited states are responsible for light emission, independent of the polarity of the contacts. This is illustrated in Fig. 4.12, showing forward and reverse mode EL spectra (the spectra are recorded at + 8 and - 20 V for forward and reverse bias operation respectively). The reverse mode EL spectrum is recorded only slightly above the onset of EL, since at relatively high electric fields devices are known to degrade rapidly, resulting in reduced light intensity before finally complete failure of the device. The similarity of EL in both operation modes proves that the reverse bias EL is not associated with a breakdown of the device at high fields, which is generally associated with plasma emission and sparks taking over from the conventional luminescence. The high-field atomic emission described in section 6.2 of this thesis was not observed for ITO/P3OT/Al LEDs, since overall fields > $3 \cdot 10^8$ V/m could not be achieved before complete breakdown of the device.

## 4.4 Dominant influence of the cathodic workfunction on rectification ratio and efficiency

In close analogy to Parkers study of IV and LV characteristics of conjugated polymer LEDs based on MEH-PPV, a variation of the top metallic electrode was applied to P3OT-based devices. As a result of band-bending at the upper
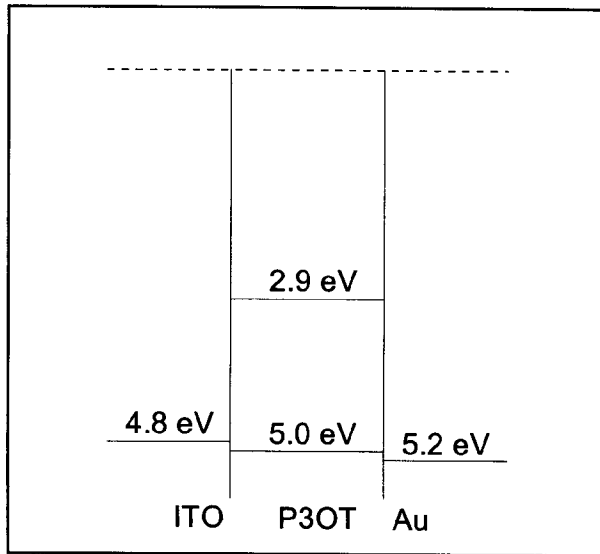
Fig. 4.13 *Relevant levels of the molecular transport bands of P3OT in relation to the Fermi level positions for ITO and Au electrodes. The HOMO level position of P3OT is located higher than the Au Fermi level, resulting in an Ohmic contact.*

electrode and the relatively high barrier for electron-injection on this side of the device, the onset-fields for EL and the efficiencies of the devices are expected to be totally different in our ITO/P3OT/Al devices.

The relevant energy levels of an ITO/P3OT/Au LED are indicated in Fig. 4.13, which shows that the workfunctions of both metallic electrodes are close to the valence band position of P3OT, while the barriers for electron injection in forward (+ on ITO) and reverse (+ on Au) mode of operation are 1.9 and 2.3 eV, respectively. These barriers are enormous compared to the injection barriers for holes in both modes of operation, which are 0.2 and 0 eV, respectively.
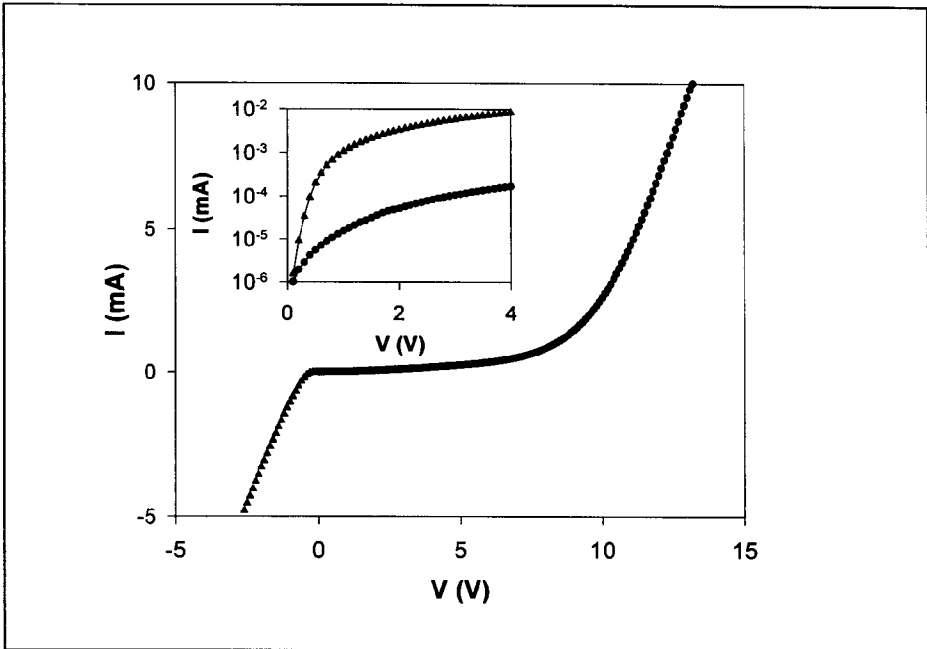
Fig. 4.14   *IV-characteristics   for   an   ITO/P3OT/Au-device.   Positive   bias corresponds to a positive polarity at the ITO-electrode. The inset shows the same data on a semi-log scale, showing the rectifying properties of the device.*

Fig. 4.14 shows the *IV*-characteristics for a 100 nm thick ITO/P3OT/Au device structure in both modes of operation. Comparison of this characteristic to the corresponding ITO/P3OT/Al (Fig. 4.9) structure shows that the highest current density at a specific voltage is now obtained in the reverse mode of operation, which is consistent with the imbalance of the workfunctions of the two electrodes indicated in Figs. 4.4 and 4.13. The inset of Fig. 4.14 shows the same data on a semilogarithmic scale, from which we can conclude that ITO/P3OT/Au devices have a rectification ratio of almost two orders of magnitude. Taking into account the different preferred modes of operation of the device for a specified set of electrodes, we conclude that upon changing the workfunction of the top electrode by only 0.9 eV the difference in rectification ratio is effectively 6 orders of magnitude. This justifies the statement that in P3OT-based LEDs the workfunction of the upper metallic electrode dominates the shape of the *IV*-characteristic, both in forward and reverse mode of operation.
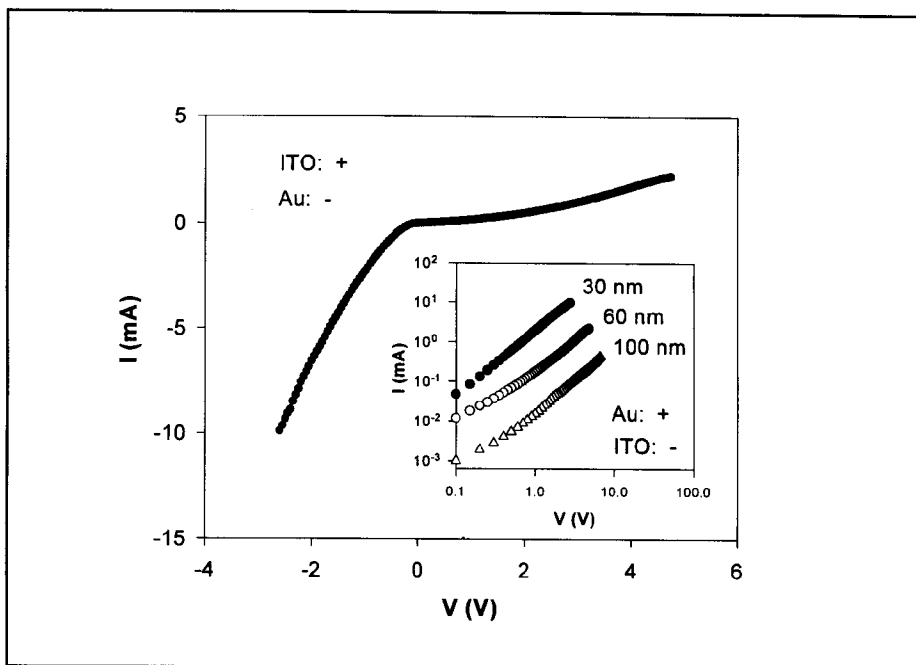
Fig. 4.15   _IV-characteristics of a device similar to that indicated in Fig. 4.14. The inset shows the IV-characteristics for 3 devices with different thicknesses of the active layer on a double-logarithmic scale._

Since we have concluded that the shape of the _IV_-characteristics of P3OT-based devices is determined by the injection barriers at the electrodes, the asymmetry of the curve in Fig. 4.14 unambiguously shows that the ITO/P3OT contact is not Ohmic, since the current density has been reduced significantly compared to an IV in which the Au/P3OT contact dominates. This explains why the _IV_-characteristic of an ITO/P3OT/Al device is injection limited due to the cathodic Schottky barrier instead of bulk limited by the P3OT-film itself. Since the height of the P3OT/Al Schottky barrier is 0.5 eV higher as the band offset at the ITO/P3OT interface, the magnitude of the hole current is determined by the cathode contact. In this configuration the ITO/P3OT contact can be regarded as 'nearly Ohmic'.

The reverse-bias characteristics of ITO/P3OT/Au structures with different thicknesses of the polymer film are analysed in more detail in Fig. 4.15 on a linear scale, and in the inset on a log-log scale. A fit to almost the complete _IV_-characteristic yields a dependence of $I \propto V^2$ for all 3 different thicknesses, as is predicted by Eq. 2.22 for space charge limited currents. This experimental observation confirms the absence of a substantial injection barrier $\phi_b > k_B T$ at the Au/P3OT interface for hole injection into the polymer film, i.e. the contact is

able to sustain the maximum allowed current density in the bulk of the low-mobility polymer. The Ohmic character of P3OT/Au contacts has also been predicted based on theoretical analysis of metal/polymer contacts by Brazovskii *et al.* [17] . Assuming $\varepsilon_r = 4$, Eq. 2.22 yields a hole-mobility μ_h of 10^{-6} cm^2/Vs for P3OT, a value which is not too different from the experimental values reported in the literature for similar materials.

The current densities in Fig. 4.14 entirely exist of holes being transported across the polymer film. The absence of an electron contribution is justified by the presence of enormous barrier heights for injection of those carriers at the metallic contacts compared to those for holes. Direct consequence is that an ITO/P3OT/Au LED does not show EL, since the low electron density in the P3OT-film does not result in significant recombination of electrons and holes.

Instead of Al top electrodes also In top contacts were used for the P3OT-devices described here. Although the workfunctions of the two metals are similar, we generally prefer to use Al. One of the problems associated with In is that it is very mobile upon deposition, and thus is likely to diffuse into the polymer film, inducing excessive doping and non-radiative quenching centres. The report of Gustafsson *et al.* [8] of changing dopant profiles upon changing the bias across these devices also leads to suspicion of mobile dopants such as In present in the film at relatively high electric fields. Esselink *et al.* [18] have shown that already under normal deposition conditions In tends to form 30 nm-diameter granules which are sensitive to clustering. Upon annealing to 160 °C for 80 min. the In-film is observed to diffuse deeply into the P3OT-film, the diffusion depth being dependent on the temperature. The same studies performed with Al-deposited metallic top-layers show that Al does not have the tendency to diffuse into the polymer film at elevated temperatures, and hence Al forms a much more stable electrode system compared to In. It is important to note that upon applying high power to those LEDs (5-10 V at currents exceeding 10 mA) similar temperatures as those in the annealing experiments can be reached; indeed it was observed that after operation for a few minutes at high power, ITO/P3OT/In devices became short-circuited, which is believed to be a direct result of In-diffusion through the polymer film. ITO/P3OT/Al devices did remain stable under identical operational conditions. In an early stage of research, we have permanently changed to using Al instead of In top electrodes.

The opposite situation is realised by changing the top electrode to a metal with a workfunction of only 2.9 eV (Ca), which perfectly connects to the molecular LUMO-level of P3OT. This should result in a maximised electron-contribution to the *IV*-characteristic of the device, while at the same time the Schottky barrier that holes face at the P3OT/Ca interface is almost as high as the P3OT bandgap (see Fig. 4.16 for the band representation of the device structure). Since the injection barrier for holes at the Ca/P3OT interface in the reverse mode of operation is very high in this case, the reverse bias current density is negligibly small. This again justifies the forward-bias picture of holes being the majority
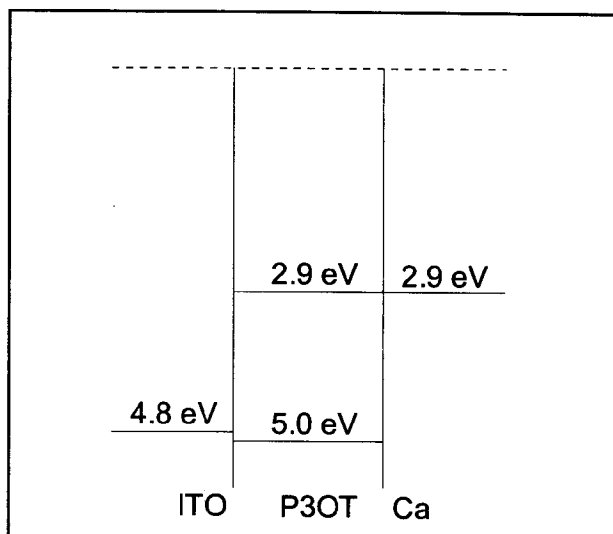
Fig 4.16 *Relevant levels of the molecular transport bands of P3OT in relation to the Fermi-level positions for ITO and Ca electrodes.*

carriers in these device structures, where the role of electrons is only to realise sufficient recombination to observe EL. The total electron contribution to the current density is so small that it can safely be neglected.

The results described here confirm the first literature studies of P3OT/Ca devices of Brown *et a.l* [15] and Greenham *et al.* [9]. Their results also show that the rectification ratios for ITO/P3OT/Ca and ITO/P3OT/In (In has the same workfunction as Al) are not that different, which is a result of a lower hole (majority) carrier contribution, not only in the forward but in the reverse mode of operation as well. The statements in Brown *et al.* [15] that the turn-on voltage for ITO/P3OT/Ca devices compared to ITO/P3OT/In devices is smaller should be refined in that respect, that it only reflects a higher injection rate for electrons at a similar voltage. Since at this voltage the hole current density in ITO/P3OT/Ca is smaller than in ITO/P3OT/Al, the turn-on voltage is indeed smaller, which justifies that already at low operation voltages significant electron-injection has been established from the Ca-contact.

The internal EL quantum efficiencies for ITO/P3OT/Al and ITO/P3OT/Ca devices are $5.0 \cdot 10^{-3}$ % and $1.6 \cdot 10^{-1}$ %, respectively. The difference between the two values is directly related to the different electron contribution to the total charge density in the polymer film. The conclusion of the former section that the top

metallic electrode in P3OT-based EL devices dominates the device *IV*-characteristics and EL-efficiencies is justified by these values. The efficiency of P3OT-based devices does not depend on the film thickness (as was also observed by Greenham *et al.* [9]); this is to be expected when all recombination is taking place in the interfacial depletion zone of the top contact, where the dominant voltage drop across the total device structure occurs. The absolute value of the voltage drop remains the same when dictated by the energy levels at the P3OT/Al interface, and is not sensitive to the negligible voltage drop across the rest of the thickness of the polymer layer.

It is noted here that the external EL efficiency of an ITO/P3OT/Ca device is among the highest efficiencies reported for P3OT-based polymeric LEDs, but that this value is still small compared to the values obtained with most PPV-derivatives. This is generally accepted, as the P3AT-films are known to have rather low PL quantum efficiencies (our measurements yield less than 1 %). The highly planar configuration of P3OT due to head-to-tail coupling of the rings in the film is believed to contribute significantly to this effect, since classical concentration quenching effects from non-emissive sites play a role. Xu *et al.* [19] have shown that increasing the concentration of non-planar head-to-head coupling increases the thiophene PL fluorescence yields, since these twisted structures are much less susceptible to
intermolecular deactivation (excimer-type excited state complexes, exciton transfer, etc.) [20].

Another factor which reduces EL yield in P3AT-devices compared to PPV-derivatives is the height of the background carrier concentration, which is known to be much higher in thiophenes than in PPVs prepared via the precursor-route (see section 4.2). Greenham *et al.* [9] confirmed this by showing that the efficiency of high carrier concentration P3AT-films ($N_A \approx 10^{-19}$ cm^{-3}) is significantly lower than in standard P3AT-based devices ($N_A \approx 10^{-16}$ cm^{-3}). The difference in luminescence efficiencies also shows up when comparing the PL quantum efficiencies of P3OT and Si-PPV-films, as is described in more detail in section 6.1.

4.5 References

[1] R.E. Gill, G.G. Malliaras, J. Wildeman, G. Hadziioannou, Adv. Mat. **6**, 132 (1994).

[2] I.D. Parker, J. Appl. Phys. **75**, 1656 (1994).

[3] S. Karg, W. Riess, V. Dyakonov, M. Schwoerer, Synth. Met. **54**, 427 (1993).

[4] U. Lemmer, S. Karg, M. Scheidler, M. Deussen, W. Riess, B. Cleve, P. Thomas, H. Bässler, M. Schwoerer, E.O. Göbel, Synth. Met. **67**, 169 (1994).

[5]   H. Antoniadis, B.R. Hsieh, M.A. Abkowitz, S.A. Jenekhe, M. Stolka, Synth. Met. **62**, 265 (1994).

[6]   H. Tomozawa, D. Braun, S. Phillips, A.J. Heeger, H. Kroemer, Synth. Met. **22**, 63 (1987).

[7]   C.S. Kuo, F.G. Wakim, S.K. Sengupta, S.K. Tripathy, J. Appl. Phys. **74**, 2957 (1993).

[8]   G. Gustafsson, M. Sundberg, O. Inganäs, C. Svensson, Journal of Molecular Electronics **6**, 105 (1990).

[9]   N.C. Greenham, A.R. Brown, D.D.C. Bradley, R.H. Friend, Synth. Met. **55-57**, 4134 (1993).

[10]   B.H. Cumpston, K.F. Jensen, Appl. Phys. Lett. **69**, 3941 (1996).

[11]   C. Väterlein, "Oligomere elektrolumineszenzdioden – Elektrische charakterisierung und optimierung", PhD-thesis, University of Würzburg, 1996.

[12]   M. Esteghamatian, G. Xu, Synth. Met. **75**, 149 (1995).

[13]   I.H. Campbell, D.L. Smith, J.P. Ferraris, Appl. Phys. Lett. **66**, 3030 (1995).

[14]   B. Workalemahu, "Electronic Properties of Junctions Between Aluminium and Doped Polyheterocycles", PhD-thesis, Linköping University (Sweden), 1996.

[15]   D. Braun, G. Gustafsson, D. McBranch, A.J. Heeger, J. Appl. Phys. **72**, 564 (1992).

[16]   D.D.C. Bradley, seminar presented at the University of California, Santa Barbara, aug 16, 1991.

[17]   S.A. Brazovskii, N.N. Kirova, Synth. Met. **55-57**, 4385 (1993).

[18]   F.J. Esselink, G. Hadziioannou, Synth. Met. **75**, 209 (1995).

[19]   B. Xu, S. Holdcroft, Macromolecules **26**, 4457 (1993).

[20]   M.R. Andersson, M. Berggren, O. Inganäs, G. Gustafsson, J.C. Gustafsson-Carlberg, D. Selse, T. Hjertberg, O. Wennerström, Macromolecules **28**, 7525 (1995).